A Swine Hind Limb Ischemia Model Useful for Testing Peripheral Artery Disease Therapeutics

Juline N. Deppen[1,2] · Sydney C. Ginn[1,2] · Na Hee Kim[2] · Lanfang Wang[2] · Ronald J. Voll[3] · Steven H. Liang[4] ·
Mark M. Goodman[3] · John N. Oshinski[1,3] · Rebecca D. Levit[2]

Abstract

Currently, there is no large animal model of sustained limb ischemia suitable for testing novel angiogenic therapeutics for peripheral artery disease (PAD) such as drugs, genes, materials, or cells. We created a large animal model suitable for efficacy assessment of these therapies by testing 3 swine hind limb ischemia (HLI) variations and quantifying vascular perfusion, muscle histology, and limb function. Ligation of the ipsilateral external and bilateral internal iliac arteries produced sustained gait dysfunction compared to isolated external iliac or unilateral external and internal iliac artery ligations. Hyperemia-dependent muscle perfusion deficits, depressed limb blood pressure, arteriogenesis, muscle atrophy, and microscopic myopathy were quantifiable in ischemic limbs 6 weeks post-ligation. Porcine mesenchymal stromal cells (MSCs) engineered to express a reporter gene were visualized post-administration via positron emission tomography (PET) in vivo. These results establish a preclinical platform enabling better optimization of PAD therapies, including cellular therapeutics, increasing bench-to-bedside translational success.

Abbreviations

ABI	Ankle-brachial index
CT	Computed tomography
EIA	External iliac artery
FBS	Fetal bovine serum
^{18}F-MFBG	^{18}F-meta-fluorobenzylguanidine
GH	Growth hormone
hNET	Human norepinephrine transporter
IGF-1	Insulin-like growth factor 1
IIA	Internal iliac artery
mGFP	mTag green fluorescent protein
MSC	Mesenchymal stromal cell
MRI	Magnetic resonance imaging
PAD	Peripheral artery disease
PBS	Phosphate-buffered saline
PET	Positron emission tomography
TOF MRA	Time-of-flight magnetic resonance angiography
HLI	Hind limb ischemia

✉ Rebecca D. Levit
rlevit@emory.edu

1   Wallace H. Coulter Department of Biomedical Engineering, Georgia Institute of Technology and Emory University, Atlanta, GA, USA

2   Division of Cardiology, Department of Medicine, Emory University School of Medicine, Atlanta, GA, USA

3   Department of Radiology and Imaging Sciences, Emory University School of Medicine, Atlanta, GA, USA

4   Department of Radiology, Massachusetts General Hospital and Harvard Medical School, Boston, MA, USA

Introduction

Peripheral artery disease (PAD) is caused by atherosclerotic arterial narrowing and leads to progressive limb symptoms including claudication, rest pain, and skeletal muscle myopathy in over 200 million people worldwide [1, 2]. Large-artery revascularization remains the only specific treatment for severe PAD; however, the anatomy and surgical risk of many patients are not amenable to these procedures [3–5]. Current medical and minimally invasive therapies fail to alleviate symptoms and prevent lower extremity amputation in up to 25% of patients with critical limb ischemia [3, 4, 6].

Bench-to-bedside translation of revascularizing PAD therapies requires studies in models beyond small animal hind limb ischemia (HLI). Major constraints of this common model, including acute vascular injury disparate from clinical disease manifestation and small muscle volumes incomparable to human leg vascular inflow and metabolic activity, lead to failure in predicting PAD patient efficacy [7–9]. Unknowns also remain regarding the optimal therapeutic delivery strategy in humans in terms of dosage, location, method, and frequency [7, 10, 11]. Therefore, many phase II and III trials showed no primary outcome efficacy vs. placebo [12–16]. JUVENTAS cited functional neovascularization in rat HLI, but no differences in major amputation nor secondary outcomes were seen with bone marrow mononuclear cells vs. placebo in humans [12, 17]. TAMARIS noted vascular growth using an FGF-1 plasmid in hamster HLI but no clinical improvements vs. placebo in amputation nor death [14, 18]. A safe, feasible starting dose for a phase I trial can be established using large animals that mimic the scale of human disease. Large animal models provide evidence for perfusion changes in the large-volume human leg and allow testing of delivery strategies with patient-applicable outcomes, equipment, and imaging modalities [7, 8, 19, 20]. Functional benefits in clinical trials also better correlate with large vs. small animal studies [8, 19].

For PAD, previous large animal HLI models have been attempted with unilateral ligations or occlusions of the external iliac artery (EIA) [21, 22], femoral artery [23–26], or EIA and internal iliac artery (IIA) [27]. These swine models have neither exhibited sustained limb dysfunction nor muscle perfusion deficits for multiple weeks post-model creation, making it difficult to assess therapeutic potency and guide clinical trial design [21–27]. Large animal optimization may be particularly beneficial for cellular therapies, which show low retention post-administration in ischemic tissue [3, 7, 10, 11, 28, 29]. Real-time localization of viable cells preclinically begins to ascertain the duration of beneficial effects in patients. Positron emission tomography (PET) reporter gene imaging improves upon other porcine-applicable techniques to assess administered cell fate as it is precise in anatomical localization, non-invasive, specific to live cells, and sensitive in detecting small cell numbers [29, 30].

The objective of this study was to create a preclinical platform to better assess the benefits and mechanisms of PAD therapeutics in swine prior to clinical trials. This platform consisted of a porcine model of sustained HLI with objective quantification of limb dysfunction, limited perfusion, myopathy, and administered cell persistence, establishing a more consistent foundation for future studies of various PAD therapies.

Methods

Additional detail is found in Online Resource 1.

Creation and Quantification of Swine HLI

Experimental timeline is shown in Fig. 1a for Yorkshire cross swine ($N = 13$; 1 castrated male, 12 females; 45–58 kg).

Limb Blood Pressure Measurements

Limb systolic blood pressure measurements were taken using an inflatable cuff (SurgiVet® Advisor®) under sedation. Ankle-brachial indices (ABIs) were calculated by dividing hind limb by ipsilateral forelimb pressures.

Catheterization and Angiography

A 5-Fr straight pigtail catheter (PERFORMA®, Merit Medical) was inserted into a sheath placed in the common carotid artery and advanced proximal to the abdominal aortic bifurcation. Contrast agent (Omnipaque™ 300 mg iodine/mL, GE Healthcare) was administered with a power injector (15 mL/s, 2 s, 500 psi) with cine angiography performed with a Philips Allura Xper FD10 X-ray system at 15 fps. Magnetic resonance angiography (MRA) was performed using a multi-slice 2D time-of-flight (TOF) sequence on a 3.0-T scanner (Siemens Medical).

HLI Induction

Following a midline abdominal incision, arteries were exposed through blunt retroperitoneal dissection. Four arterial ligation strategies were attempted (Fig. 1b):

Single ligation. Right EIA immediately distal to the aorta ($N = 1$) or at the saphenous/popliteal femoral bifurcation ($N = 1$)
*Double ligation.* Right EIA and right IIA ($N = 5$)
Triple ligation. Right EIA and bilateral IIAs ($N = 6$)

All ligations were performed with 0-silk sutures with proximal or distal transfixation sutures (4-0 prolene) facing excision sites (Fig. 1b, X's). After confirming the absence of bleeding, incisions were closed in layers with Vicryl and/or PDS sutures. Post-ligation angiograms (sample in Fig. 1c) were performed as above.

Gait Analysis

Swine gait patterns were quantified pre- and post-ligation with a 16-ft custom animal walkway system (Tekscan, Inc.) and analyzed with accompanying software. Multiple trotting passes (2–11) were used for each session with data averaged to obtain one value per animal at each time point.
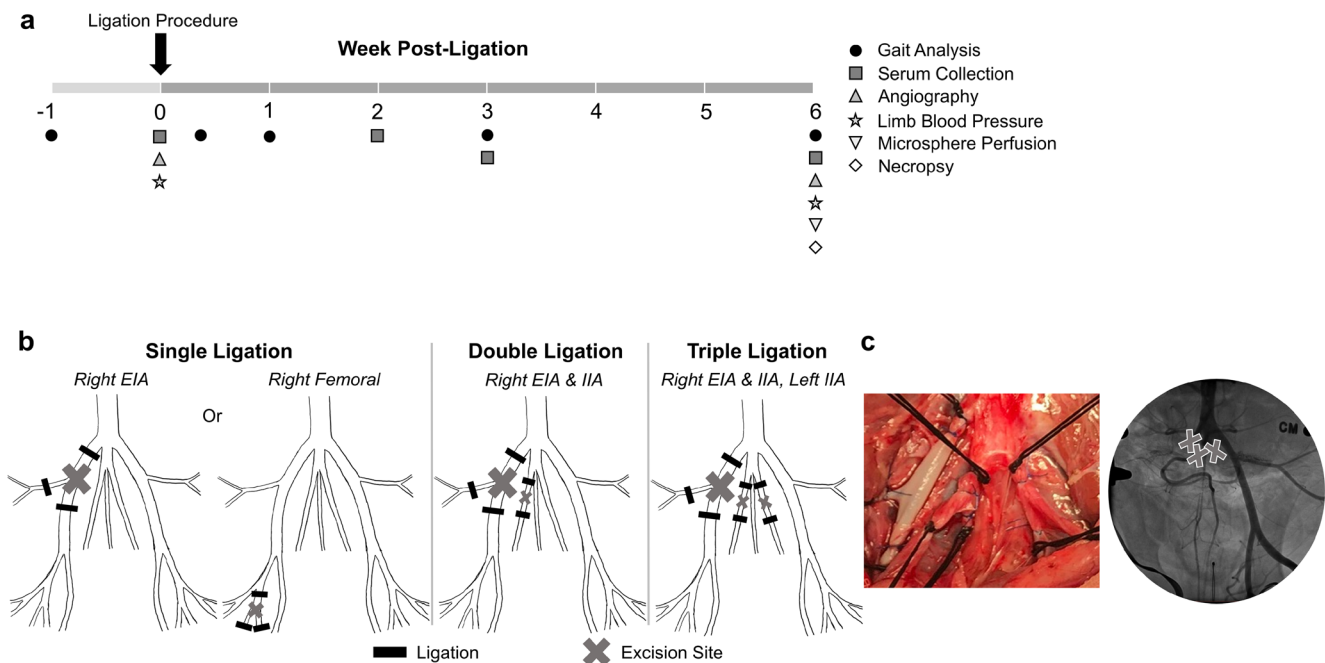
Fig. 1 Overview of experimental strategies for pig hind limb ischemia (HLI). **a** Timeline for creation and characterization of HLI model variations. **b** Swine pelvic arteries with ligation and excision locations for attempted HLI models. **c** Representative surgical image (post-ligation, pre-excision) and post-procedure angiogram (after contrast injection in the distal aorta) for the triple ligation model. EIA, external iliac artery; IIA, internal iliac artery

Serum Analysis

Creatine kinase activity in serum was determined using a clinical assay (Vet Axcel® Chemistry Analyzer).

Terminal Procedure and Analysis

Six weeks post-ligation, swine underwent catheterization, blood pressure measurements, and angiography as above. Two 5-Fr pigtail catheters were inserted into the carotid sheath with the additional catheter positioned in the left ventricle for microsphere infusion. Collateral frame counting [31] and arterial diameters [21] were measured using the visible aorta as the parent vessel.

Microsphere Perfusion Assessment, Euthanasia, and Tissue Collection

Fluorescent polystyrene microspheres (4×10^6, 15 μm, Molecular Probes®) were injected into the left ventricle over 45 s, and a reference blood sample was withdrawn concurrently from the aortic catheter (4 mL/min, 5-min duration) into a heparin-containing glass syringe. To measure hyperemic hind limb perfusion, an adenosine bolus (12 mg) was administered through the aortic catheter immediately prior to administration of microspheres of a second color.

Swine under deep anesthesia were euthanized using a lethal dose of potassium chloride. Perfusion samples were collected from throughout each hind limb muscle. After autolyzing for 2 weeks, individual muscle samples were ground together, and 1–3 g of the mixture were digested alongside reference blood samples as previously described using a 50 °C bacterial shaker [32]. Fluorimetry was performed via a multi-mode microplate reader (Synergy™ H1, Biotek Instruments, Inc.).

Wet weights of individually dissected hind limb muscles were recorded. Muscle histological samples were collected from similar locations in ischemic and non-ischemic limbs and fixed in 10% neutral-buffered formalin.

Histology

Masson's trichrome and immunofluorescence staining for dystrophin (Abcam ab15277) were performed. MyoVision software was used for muscle fiber quantification [33].

MSC PET Imaging via Human Norepinephrine Transporter (hNET) and ¹⁸F-MFBG

Lentiviral Vector Construction, Transduction, and Analysis

A custom lentiviral vector, hNET-P2A-mGFP-T2A-Blast, was cloned containing hNET, mGFP, and an antibiotic resistance gene and packaged using 293T cells (ATCC®). P2-P3

porcine MSCs were transduced in T75 flasks using 2 mL of viral supernatant and 8 μg/mL polybrene (Sigma-Aldrich® AL-118). Antibiotic selection with 2 μg/mL blasticidine S hydrochloride (Sigma-Aldrich® 15205) commenced 48 h post-transduction and continued throughout culture. hNET expression was assessed using immunofluorescence staining (anti-human NET primary antibody; mAb Technologies NET17-1).

^{18}F-MFBG Uptake and PET Visualization

P3-P5 MSCs were incubated with ^{18}F-MFBG (5 μCi/200,000 cells, synthesized using a spirocyclic iodonium(III) ylide precursor [34, 35]) for 30 min at 37 °C followed by 2 washes with cold PBS. Remaining radioactivity in PBS-resuspended cell pellets was measured in a Packard Cobra II Auto-Gamma counter with raw counts decay-corrected. Alginate-encapsulated [28] or free porcine MSCs were injected subcutaneously over rat hind limbs. Imaging was conducted 1 day later after tail vein injection of ^{18}F-MFBG (250 μCi). Scanning was completed with an Inveon micro-PET/CT scanner (Siemens Medical) for 4 5-min PET frames and attenuation correction via CT.

Statistical Analysis

Analyses were performed with GraphPad Prism 8 for model variation cohorts with $N > 2$. Values are presented as mean ± standard deviation (SD). Data for the same procedure over time were compared using a one-way repeated measures ANOVA or two-tailed paired t-test (> 2 or 2 time points, respectively). Ischemic vs. non-ischemic limb values for one model were compared with a two-tailed ratio paired t-test. Tracer uptake was compared via a one-way ANOVA. All ANOVAs were followed by Tukey's post hoc analyses. P-values < 0.05 were considered significant.

Results

HLI Induction via Triple Ligation in Older Swine Produced Sustained Functional Abnormalities

All animals underwent successful surgical ligation and survived for 6 weeks (Fig. 1b, c). Postoperative abdominal incision complications included superficial infection in 1 animal treated with antibiotics and a hernia in 1 pig successfully repaired 10 days post-ligation; these events did not impact perioperative data collection nor results. Gait changes manifested similarly in the 4 days following HLI induction for EIA, double, and triple ligation model variations as quantified with a pressure-sensitive walkway system designed to detect differences in strike patterns of trotting animals. These

differences from pre-ligation involved a reduction in maximum stance forces, shortened stance times, and smaller hoof walkway contact areas for ischemic relative to unaffected hind limbs (Fig. 2a–c). By some measure, femoral single ligation caused a compensatory gait change manifesting with an opposite trend in stance times and contact areas (Fig. 2a). Gait patterns normalized for all animals undergoing single ligation and 4 of 5 pigs subjected to double ligation by 1 week post-ligation (Fig 2a, b). One animal in the double ligation cohort experienced prolonged surgery time and showed sustained ischemic limb functional deficits for 6 weeks (Fig. 2b squares).

Swine subjected to triple ligation HLI stratified into two separate cohorts based upon their age at the time of ligation (Fig. 2c). Data are shown separating the triple ligation cohort into older and younger pigs which differed by approximately 5 kg in weight and 1.5 weeks of age at model creation. Quantified gait dysfunction for younger pigs returned to baseline within 3 weeks post-ligation. Older pigs undergoing triple ligation sustained gait parameter changes different from baseline for 6 weeks after model creation (ischemic/non-ischemic maximum force ratio 0.534 ± 0.36 vs. 1.04 ± 0.08 pre-ligation, $p < 0.01$; ischemic/non-ischemic stance time ratio 0.864 ± 0.08 vs. 1.03 ± 0.05 pre-ligation, $p < 0.01$; Fig. 2c). Pigs undergoing this procedure were visibly limping throughout the study, with 3 of 4 unable to walk unassisted on days 1–4. Importantly, there was no visible limb necrosis for this or any model variation. These animals exhibited normal weight gain (Supplementary Fig. 1) and remained qualitatively healthy overall, allowing their continued study participation. Ligation of three pelvic arteries induces qualitative ischemic limb functional changes for 6 weeks that can be objectively quantified with a walkway system.

Lower Extremity Angiography Documented Arterial Remodeling in All HLI Models

Angiography performed 6 weeks post-ligation revealed intact ligation sites with reconstitution of distal blood flow via collateral vessels in all animals (Fig. 3a). Flow reconstitution could also be observed for the EIA single ligation animal via TOF MRA (Supplementary Fig. 2). Arteriogenesis occurred in every non-ligated major pelvic artery for older pigs in the triple ligation cohort ($p < 0.05$ for all diameters pre- vs. 6 weeks post-ligation, Fig. 3b and Supplementary Fig. 3a). Other HLI model variations also led to arteriogenic remodeling in some, but not all, non-ligated arteries, especially those closest to the ligation sites (Supplementary Fig. 3a). Additionally, there was an increase in the number of frames (and thus, time) needed for dye to appear in distal portions of ligated arteries for older vs. younger pigs in the triple ligation cohort, but findings did not reach statistical significance (Fig. 3c).
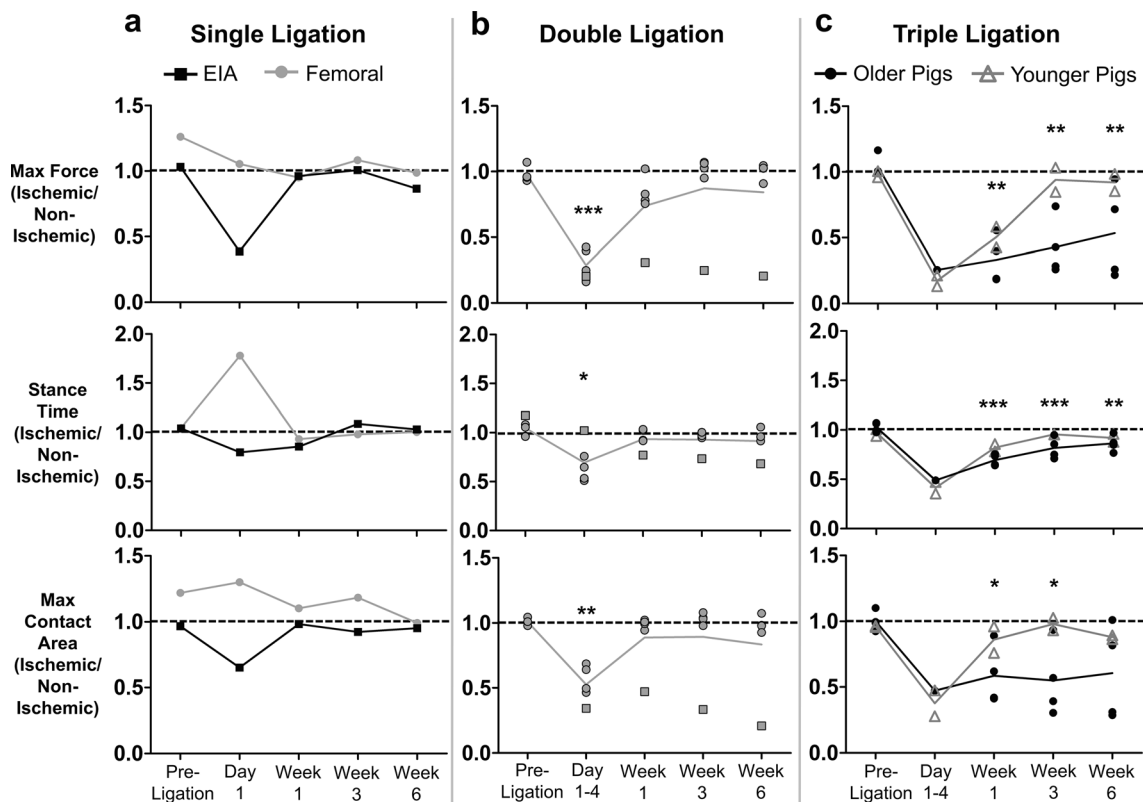
Fig. 2 Limb functional deficits were sustained for 6 weeks for the most severe ligation strategy in older pigs. Gait data collected for single, double, and triple ligation HLI model variations (**a**–**c**, respectively) with a pressure-sensing animal walkway system at key time points pre- and post-ligation. Each point represents one pig at one time point. Lines connect group means. ***$p < 0.001$, **$p < 0.01$, *$p < 0.05$ vs pre-ligation

These data suggest that ischemia-induced macrovascular remodeling occurred that potentially varied in older compared to younger swine.

Triple Ligation HLI Caused Depressed ABIs and Impaired Vasodilatory Muscle Perfusion in Older Pigs

As the triple ligation procedure in older pigs was the most successful strategy to induce sustained, consistent HLI, all remaining data is presented for this cohort only; data for other variations is in Supplementary Fig. 3. The ratio of systolic blood pressures in ischemic hind limbs relative to the ipsilateral forelimb (correlative to ABI) was depressed 6 weeks post-ligation compared to pre-ligation (0.691 ± 0.166 vs. 1.02 ± 0.193, $p < 0.01$; Fig. 4a).

We next investigated muscle perfusion in ischemic and normal limbs using microspheres. Under resting conditions, microvascular perfusion in ischemic relative to non-ischemic limb muscles was not depressed in the triple ligation cohort in the three muscle compartments investigated (Fig. 4b, top; Supplementary Fig. 4). To mimic physiologic exercise-induced hyperemia, adenosine was infused into the distal aorta. Under these conditions, perfusion deficits were seen in hamstring (63.1 ± 27.4 mL/

min 100 g vs. 108.5 ± 53.3 mL/min 100 g in non-ischemic, $p < 0.01$) and distal posterior (68.0 ± 60 mL/min 100 g vs. 152.3 ± 74.2 mL/min 100 g in non-ischemic, $p < 0.05$) but not distal anterior (87.6 ± 38.3 mL/min 100 g vs. 115.9 ± 64.4 mL/min 100 g in non-ischemic, $p > 0.05$) hind limb muscle compartments (Fig. 4b, bottom). Flow reserve in ischemic limb hamstring muscles, defined as fold change in perfusion post- vs. pre-adenosine delivery, was also significantly impaired (2.815 ± 1.40 in non-ischemic vs. 1.16 ± 0.429 in ischemic limb, $p < 0.05$; Fig. 4c). Adenosine-induced perfusion deficits were not significant in animals undergoing double ligation (Supplementary Fig. 3c). Thus, blood pressure and hyperemic muscle perfusion deficiencies were sustained in triple ligation HLI for at least 6 weeks.

Ischemic Limb Myopathy Persisted in Older Pigs After Triple Ligation

Gross muscle atrophy (depressed muscle mass to body mass ratios) existed in ischemic vs. non-ischemic hind limbs 6 weeks post-triple ligation for hamstring (12.6 ± 0.562 vs. 10.3 ± 0.534 g/kg, $p < 0.05$) and distal anterior (0.453 ± 0.0231 vs. 0.335 ± 0.0423 g/kg, $p < 0.05$) but
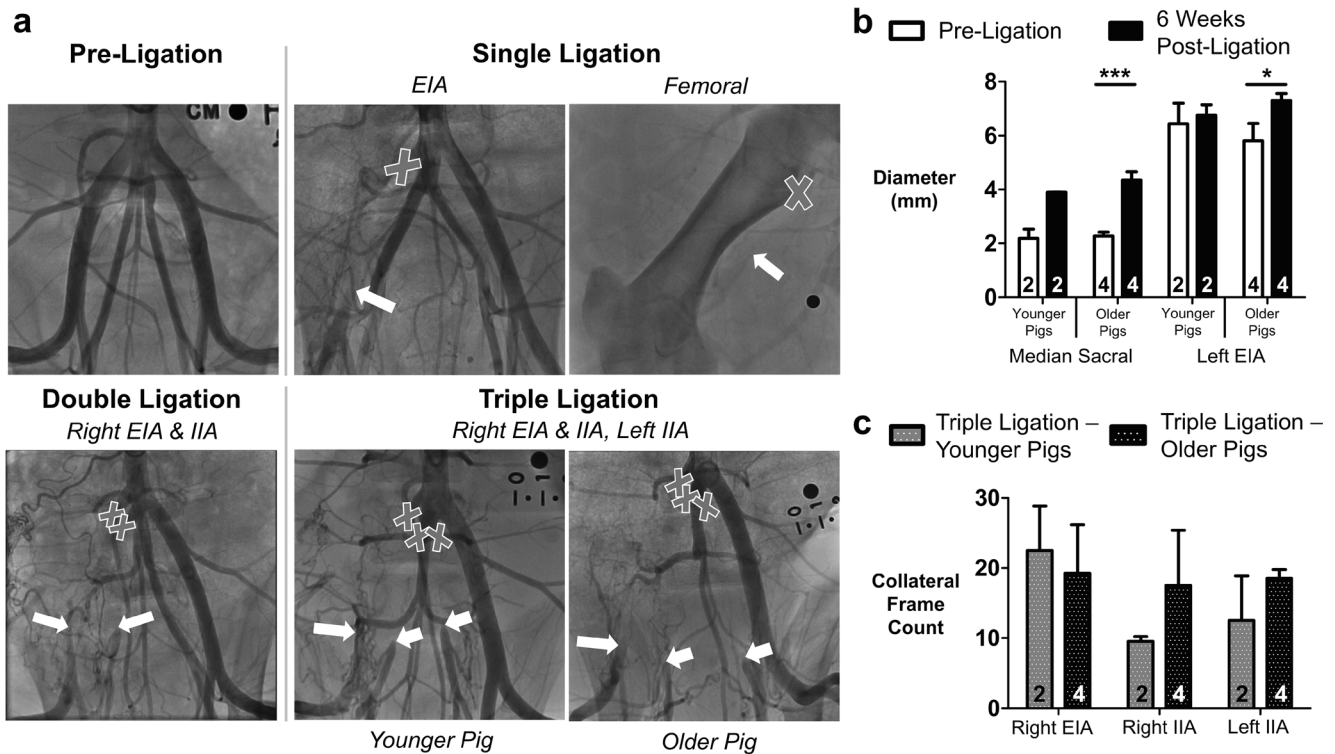
Fig. 3 Aortic angiography reveals arteriogenic remodeling and impaired collateralization in older pigs 6 weeks post-triple ligation. **a** Still images from cine angiograms after contrast injection in the distal aorta prolonged for collateral filling. X's indicate ligation sites, and white arrows denote reconstitution of distal flow via collateral vessels. **b** Non-ligated arterial diameters 6 weeks post- and pre-ligation for HLI model variations. Statistics shown for variations with $N > 2$. **c** Collateral frame count for restoration of blood flow in distal portions of ligated arteries 6 weeks post-ligation (number of cineframes required for contrast media to reach the recipient artery); p = ns. Numbers on bars, N/group. Error bars, SD. EIA, external iliac artery; IIA, internal iliac artery. ***$p < 0.001$, *$p < 0.05$

not distal posterior (3.04 ± 0.374 vs. 1.90 ± 0.617 g/kg, $p = 0.0981$) compartments (Fig. 5a). Muscle loss was detected only in the distal posterior compartment for swine undergoing double ligation (Supplementary Fig. 5). When examining specific muscles in these compartments, there was a non-significant trend toward myofiber atrophy in gastrocnemius (3519 ± 750 vs. 1921 ± 1125 μm^2, $p = 0.108$), semimembranosus (3199 ± 278 vs. 2749 ± 232 μm^2, $p = 0.170$), and peroneus tertius (3569 ± 720 vs. 2623 ± 882 μm^2, $p = 0.129$) muscles (Fig. 5b, c, minimal Feret's diameters in Supplementary Fig. 6). Ischemic myofibers also qualitatively displayed increased size heterogeneity. Select muscles analyzed in other HLI models did not display myofiber atrophy (Supplementary Fig. 6). Fibrosis was seen surrounding and within muscle fibers in focal areas of ischemic hind limb muscles (Fig. 5d). Creatine kinase, a muscle damage marker measured in a subset of animals, was elevated 2 weeks post-ligation (2442 ± 1027 vs. 544 ± 14.9 U/L pre-ligation, $p = 0.321$), then decreased throughout the 6-week study period (1509 ± 1194 U/L at week 6; Fig. 5e). Persistent elevation in some animals indicates ongoing muscle injury. Taken together, these data indicate that persistent myopathy is induced by triple ligation HLI.

PET Reporter Gene Imaging Tracked MSC Survival and Localization

To explore the possible use of this model in the preclinical development of PAD cell therapies, we applied a system for the non-invasive tracking of delivered cells. Bone marrow-derived porcine MSCs were transduced with a custom lentiviral vector, hNET-P2A-mGFP-T2A-Blast (Fig. 6a), leading to expression of hNET and GFP (hNET cells in Fig. 6b and Supplementary Fig. 7). hNET expression enables cellular uptake of specific PET tracers [36, 37]. Our transduced cells could uptake the NET-specific ^{18}F-MFBG reporter probe in vitro (23.2 ± 19.1 vs. 1.8 ± 0.4% added activity/10^6 cells in non-transduced porcine MSCs, $p = 0.0654$; Fig. 6c) and be visualized after administration freely or in alginate capsules in vivo via PET after intravenous ^{18}F-MFBG injection (Fig. 6d). This system may be useful for the longitudinal tracking of cell therapies in large animal and human trials.

Discussion

These data establish a porcine model of HLI with quantifiable deficits in limb function, ABI, muscle perfusion, and
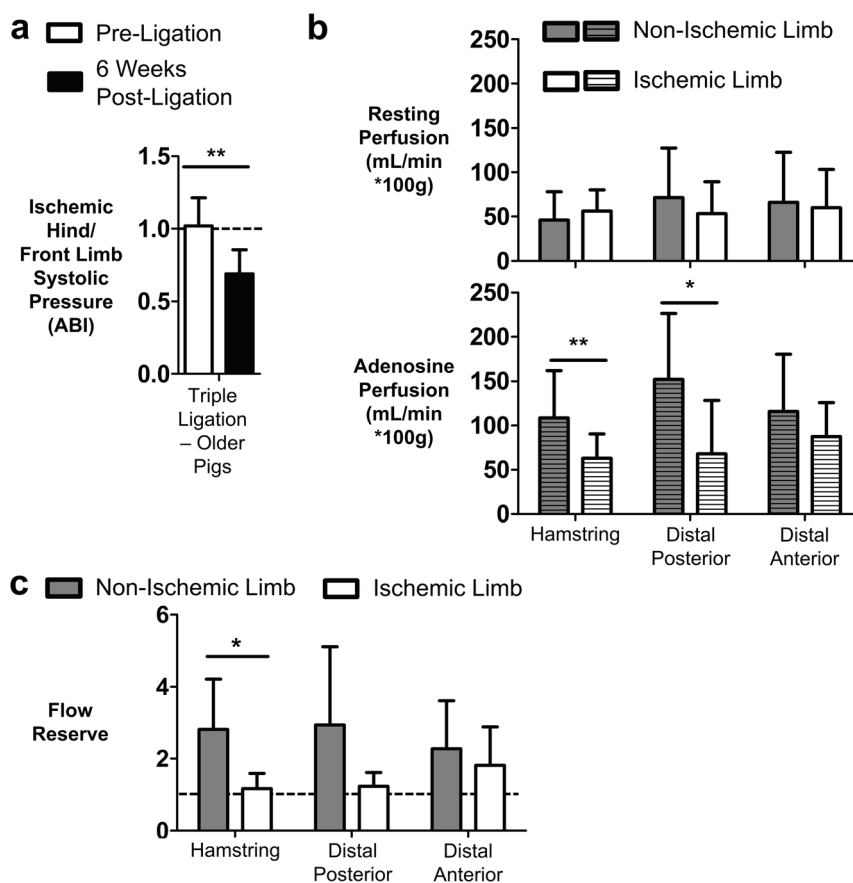
Fig. 4 Blood pressure and hyperemic muscle perfusion deficits exist for triple ligation in older pigs. **a** Ischemic hind limb ankle-brachial indices (ABIs) 6 weeks post- vs. pre-model creation. **b** Muscle microvascular perfusion 6 weeks post-HLI establishment. Ischemic and non-ischemic mean hind limb muscle compartment perfusion in resting (−adenosine, top) and hyperemic (+adenosine, bottom) states. **c** Perfusion reserve in response to adenosine in ischemic vs. non-ischemic hind limb muscle compartments 6 weeks post-ligation. $N = 4$. Error bars, SD. $**p < 0.01$, $*p < 0.05$

myopathy at least 6 weeks after ligation of 3 pelvic arteries (EIA and both IIAs) [2, 38]. Additionally, a method was demonstrated for tracking the persistence and anatomical distribution of viable cellular therapeutics non-invasively over time in this and other large animal disease models via PET. This model allows for testing of PAD therapeutics on a human scale which may more accurately predict efficacy and allow for dosage titration and administration strategy exploration prior to patient translation.

This durable swine HLI model improved upon previous models by demonstrating sustained gait disturbances and perfusion deficiencies indicative of PAD through clinically relevant and quantitative metrics [39, 40]. Producing lasting HLI in swine has been challenging, partially due to young animals' robust endogenous angiogenic/arteriogenic adaptation to acute arterial obstruction [9]. Previous HLI models in healthy juvenile/adolescent swine or adult minipigs noted robust collateralization, limiting ischemia severity and duration post-ligation [21–27]. Peripheral atherosclerosis has also been established in swine but is costly [41]. Through our approach, the most severe HLI model ligation strategy yet attempted, we

achieve sustained functional abnormalities with preservation of overall animal health. These characteristics allow for longitudinal assessment of efficacy without lameness, making this model ideal for preclinical testing of novel PAD therapeutics.

We were also able to recapitulate PAD-representative hemodynamic deficiencies and myopathy from previous HLI model variations yet also quantify microvascular perfusion deficiencies in specific anatomical muscle compartments during hyperemia [21, 27]. In PAD patients, the peripheral circulation cannot meet the metabolic demands of the exercising leg musculature, leading to exertional limb symptoms [1, 7]. Rest symptoms are present only in late-stage disease due to low baseline muscle perfusion and metabolic activity [1, 7]. Infusion of adenosine, a pharmacological vasodilator and key endogenous metabolite in active muscle, increases muscle perfusion to a level comparable to moderate- to high-intensity exercise [7, 42]. Using adenosine-induced hyperemia, we increased porcine limb muscle perfusion similarly to treadmill exercise and demonstrated that our final HLI model reproducibly recapitulates exercise-induced perfusion
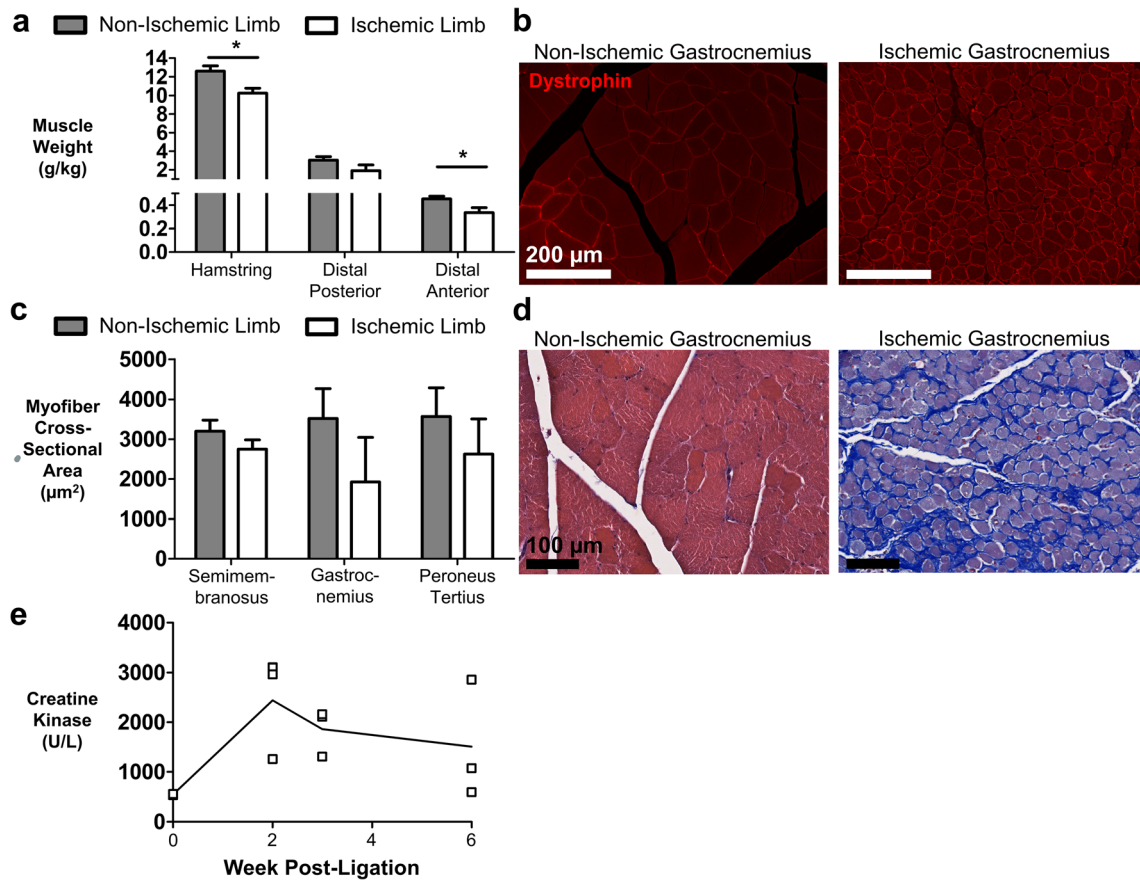
Fig. 5 A triple ligation HLI strategy in older pigs induces lasting muscle damage and macroscopic and microscopic myopathy after 6 weeks. **a** Body weight-normalized average muscle compartment wet weights in ischemic and non-ischemic hind limbs. $N = 4$. **b** Representative dystrophin immunofluorescence images. **c** Myofiber cross-sectional area measurements for sample muscles stained as in b from hamstring (semimembranosus), distal posterior (gastrocnemius), and distal anterior (peroneus tertius) compartments. $N = 4$, 3 sections/muscle, 5 images/section; p = ns for ischemic vs. non-ischemic limbs. **d** Masson's trichrome staining of representative gastrocnemii sections. **e** Serum creatine kinase. Each point represents one pig at one time point. Lines connect group means; p = ns. Error bars, SD. *$p < 0.05$

deficits characteristic of PAD [1, 43]. This attenuated vascular reserve response can be attributed to low vessel numbers, impaired or exhausted distal arteriolar dilatation capacity, and/or muscle nitric oxide, reactive oxygen species, or inflammatory activation [1, 5, 44]. Thus, this model is also well-suited for characterization of PAD therapies aiming to augment perfusion on a human-applicable scale.

When testing HLI ligation strategies, we noticed strikingly different injury severities in pigs that differed by 2 weeks in age. This effect may be due to hormonal changes. Juvenile swine used ranged in age from 15 ("younger") to 16.5–17 weeks ("older"). Porcine growth increases from birth through sexual maturity at 4–6 months, contrasting with human growth rate decline post-infancy with an adolescent spurt [45]. Serum growth hormone (GH) levels decline with increasing age between 15 and 19 weeks [46]. GH initiates the generation of insulin-like growth factor 1 (IGF-1) in the liver and other tissues. GH and IGF-1 participate in multiple facets of the collateral vessel formation, remodeling, and

arteriogenesis processes in ischemia. These include endothelial nitric oxide production and inflammation, redox stress regulation, and smooth muscle cell proliferation, and extracellular matrix remodeling [47]. The GH receptor gene is also hypoxia-inducible [48]. The changing GH and IGF-1 levels in older swine may account for the impaired revascularization in this study. These findings underscore the importance of close attention to animal age when using pigs to study PAD or other vascular diseases and the potential for future studies on this subject.

In addition to a representative disease model, longitudinal in vivo tracking of investigational PAD therapeutics in large animals can enhance preclinical evaluation and optimization. Viability and washout of cell and other therapies remain significant problems [11, 30, 49]. Post-mortem histology and labeling for MRI detection can monitor persistence but misrepresent cell numbers and viability [29, 30]. Our successful adaptation of PET reporter gene imaging with hNET/^{18}F-MFBG for biomaterial-encapsulated and free MSCs in limbs
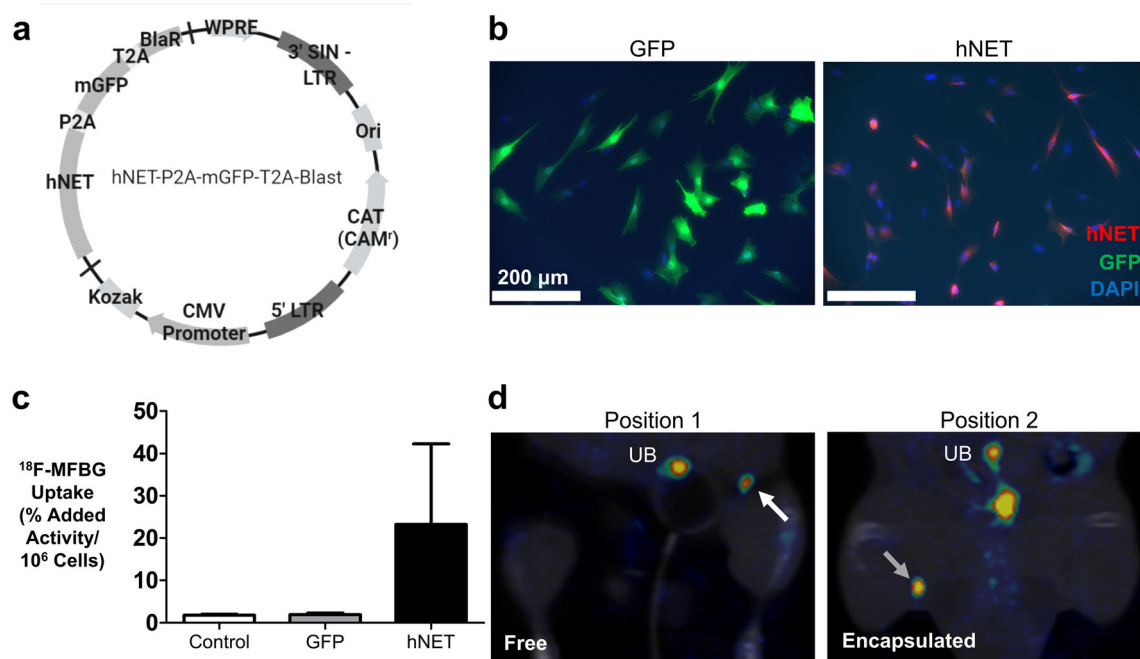
Fig. 6 The hNET/^{18}F-MFBG reporter/probe system is applicable for PET imaging of porcine MSCs. **a** Structure of lentiviral vector construct hNET-P2A-mGFP-T2A-Blast. P2A/T2A, 2A self-cleaving peptide sequences; mGFP, mTagGFP; BlaR, blasticidine resistance gene. **b** hNET expression in hNET MSCs (porcine MSCs transduced with hNET-P2A-mGFP-T2A-Blast) via immunofluorescence staining after blasticidin selection. GFP, GFP vector-transduced porcine MSCs. **c** In vitro uptake of ^{18}F-MFBG in control, GFP, and hNET MSCs. p = ns. Control, non-transduced swine MSCs. Data presented from 4 independent tracer synthesis experiments with combined cells from 2 to 3 animals. **d** ^{18}F-MFBG PET/CT imaging showing accumulation of radioactivity of subcutaneous hNET MSCs 1 day post-administration freely (white arrow) and in alginate capsules (gray arrow). hNET, human norepinephrine transporter; GFP, green fluorescent protein; ^{18}F-MFBG, ^{18}F-meta-fluorobenzylguanidine; UB, urinary bladder

is a novel, safe, high-resolution tracking approach that can be applied in future large animal efficacy studies and clinical trials [36, 37].

Several inherent limitations exist within these studies. Our use of acute healthy vessel ligation differs from the chronic atherosclerotic disease progression in PAD [9]. However, our triple ligation strategy improves upon previous acute-onset swine models as quantifiable HLI persisted for at least 6 weeks. This allows for therapeutic delivery and assessment after post-surgery compensation stabilizes, minimizing non-specific effects and enhancing clinical translation [9]. The swine used for our studies also did not possess PAD-characteristic comorbidities that can influence vascular remodeling [7, 9, 11, 21]. Young, domestic, genetically diverse pigs are less costly than swine of special breeds (Yucatan, Ossabaw), bred to express genetic mutations, and/or fed to induce metabolic syndrome, atherosclerosis, or diabetes mellitus [21, 41]. This model's accessibility may allow for studies with larger sample sizes in more diverse subjects, making results more robust and predictive of patient outcomes. Another limitation of this study is the small sample sizes stemming from exploration of 4 porcine HLI model variations. Increased subject numbers could better define age-dependent ischemic limb deficits. Additional functional insights could be gained by incorporating analyses of biomechanical walking

kinematics, more exhaustive activity, and/or hyperemic ABI. Additionally, because the microsphere perfusion method cannot be applied clinically, future studies could correlate our measurements with non-invasive muscle imaging modalities such as MRI explored here (Supplementary Fig. 2) [13, 26, 42].

We created a translational platform for large animal preclinical efficacy studies of PAD therapeutics. Our swine model using triple ligation of both IIAs and ipsilateral EIA creates long-lasting, quantifiable functional deficits as well as muscle and vascular deficiencies characteristic of PAD. We also demonstrate a technique for non-invasive cell viability and retention tracking via PET. Together, these tools enable assessment of new therapeutics and provide validation for clinical translation, ultimately improving care for PAD patients.

J. of Cardiovasc. Trans. Res. (2021) 14:1186–1197

1195

JND, SCG, NHK, LW, RJV, and JNO. Methodology: JND, RJV, SHL, MMG, JNO, and RDL. Project administration: MMG and RDL. Resources: LW, SHL, and MMG. Supervision: RDL. Visualization: JND and JNO. Writing—original draft preparation: JND. Writing—review and editing: JND, SCG, NHK, LW, RJV, MMG, JNO, and RDL.

Declarations

Ethical Approval No human studies were performed. All institutional and national guidelines for laboratory animal care and use were followed and approved by institutional committees at T3 Labs and Emory University for swine and rat studies, respectively.

Competing interests The authors declare no conflicts of interest.

References

1. Hamburg, N. M., & Creager, M. A. (2017). Pathophysiology of intermittent claudication in peripheral artery disease. *Circulation Journal, 81*(3), 281–289. https://doi.org/10.1253/circj.CJ-16-1286.

2. Pipinos, I. I., Judge, A. R., Selsby, J. T., Zhu, Z., Swanson, S. A., Nella, A. A., et al. (2007). The myopathy of peripheral arterial occlusive disease: part 1. Functional and histomorphological changes and evidence for mitochondrial dysfunction. *Vascular and Endovascular Surgery, 41*(6), 481–489. https://doi.org/10.1177/1538574407311106.

3. Suzuki, J., Shimamura, M., Suda, H., Wakayama, K., Kumagai, H., Ikeda, Y., et al. (2016). Current therapies and investigational drugs for peripheral arterial disease. *Hypertension Research, 39*(4), 183–191. https://doi.org/10.1038/hr.2015.134.

4. Gerhard-Herman, M. D., Gornik, H. L., Barrett, C., Barshes, N. R., Corriere, M. A., Drachman, D. E., et al. (2017). 2016 AHA/ACC guideline on the management of patients with lower extremity peripheral artery disease: executive summary: a report of the American College of Cardiology/American Heart Association Task Force on Clinical Practice Guidelines. *Circulation, 135*(12), e686–e725. https://doi.org/10.1161/cir.0000000000000470.

5. Cooke, J. P., & Chen, Z. (2015). A compendium on peripheral arterial disease. *Circulation Research, 116*(9), 1505–1508. https://doi.org/10.1161/circresaha.115.306403.

6. Jones, W. S., Dolor, R. J., Hasselblad, V., Vemulapalli, S., Subherwal, S., Schmit, K., et al. (2014). Comparative effectiveness of endovascular and surgical revascularization for patients with peripheral artery disease and critical limb ischemia: systematic review of revascularization in critical limb ischemia. *American Heart Journal, 167*(4), 489–498.e487. https://doi.org/10.1016/j.ahj.2013.12.012.

7. Cooke, J. P., & Losordo, D. W. (2015). Modulating the vascular response to limb ischemia: angiogenic and cell therapies.

8. USFDA (2010). Guidance for industry: cellular therapy for cardiac disease. In U.S. D.o.H.a.H. Services (Ed.). Rockville, .

9. Waters, R. E., Terjung, R. L., Peters, K. G., & Annex, B. H. (2004). Preclinical models of human peripheral arterial occlusive disease: implications for investigation of therapeutic agents. *Journal of Applied Physiology (Bethesda, MD: 1985), 97*(2), 773–780. https://doi.org/10.1152/japplphysiol.00107.2004.

10. Hassanshahi, M., Khabbazi, S., Peymanfar, Y., Hassanshahi, A., Hosseini-Khah, Z., Su, Y. W., et al. (2019). Critical limb ischemia: current and novel therapeutic strategies. *Journal of Cellular Physiology.* https://doi.org/10.1002/jcp.28141.

11. Qadura, M., Terenzi, D. C., Verma, S., Al-Omran, M., & Hess, D. A. (2018). Concise review: cell therapy for critical limb ischemia: an integrated review of preclinical and clinical studies. *Stem Cells, 36*(2), 161–171. https://doi.org/10.1002/stem.2751.

12. Teraa, M., Sprengers, R. W., Schutgens, R. E., Slaper-Cortenbach, I. C., van der Graaf, Y., Algra, A., et al. (2015). Effect of repetitive intra-arterial infusion of bone marrow mononuclear cells in patients with no-option limb ischemia: the randomized, double-blind, placebo-controlled Rejuvenating Endothelial Progenitor Cells via Transcutaneous Intra-arterial Supplementation (JUVENTAS) trial. *Circulation, 131*(10), 851–860. https://doi.org/10.1161/circulationaha.114.012913.

13. Perin, E. C., Murphy, M. P., March, K. L., Bolli, R., Loughran, J., Yang, P. C., et al. (2017). Evaluation of cell therapy on exercise performance and limb perfusion in peripheral artery disease: the CCTRN Patients with Intermittent Claudication Injected with ALDH Bright Cells (PACE) trial. *Circulation.* https://doi.org/10.1161/circulationaha.116.025707.

14. Belch, J., Hiatt, W. R., Baumgartner, I., Driver, I. V., Nikol, S., Norgren, L., et al. (2011). Effect of fibroblast growth factor NV1FGF on amputation and death: a randomised placebo-controlled trial of gene therapy in critical limb ischaemia. *The Lancet, 377*(9781), 1929–1937. https://doi.org/10.1016/S0140-6736(11)60394-2.

15. Creager, M. A., Olin, J. W., Belch, J. J., Moneta, G. L., Henry, T. D., Rajagopalan, S., et al. (2011). Effect of hypoxia-inducible factor-1alpha gene therapy on walking performance in patients with intermittent claudication. *Circulation, 124*(16), 1765–1773. https://doi.org/10.1161/circulationaha.110.009407.

16. Poole, J., Mavromatis, K., Binongo, J. N., Khan, A., Li, Q., Khayata, M., et al. (2013). Effect of progenitor cell mobilization with granulocyte-macrophage colony-stimulating factor in patients with peripheral artery disease: a randomized clinical trial. *JAMA, 310*(24), 2631–2639. https://doi.org/10.1001/jama.2013.282540.

17. Yoshida, M., Horimoto, H., Mieno, S., Nomura, Y., Okawa, H., Nakahara, K., et al. (2003). Intra-arterial bone marrow cell transplantation induces angiogenesis in rat hindlimb ischemia. *European Surgical Research, 35*(2), 86–91. https://doi.org/10.1159/000069401.

18. Caron, A., Michelet, S., Caron, A., Sordello, S., Ivanov, M. A., Delaere, P., et al. (2004). Human FGF-1 gene transfer promotes the formation of collateral vessels and arterioles in ischemic muscles of hypercholesterolemic hamsters. *The Journal of Gene Medicine, 6*(9), 1033–1045. https://doi.org/10.1002/jgm.594.

19. Tompkins, B. A., Balkan, W., Winkler, J., Gyongyosi, M., Goliasch, G., Fernandez-Aviles, F., et al. (2018). Preclinical studies of stem cell rherapy for heart disease. *Circulation Research, 122*(7), 1006–1020. https://doi.org/10.1161/circresaha.117.312486.

20. Harding, J., Roberts, R. M., & Mirochnitchenko, O. (2013). Large animal models for stem cell therapy. *Stem Cell Research & Therapy, 4*(2), 23. https://doi.org/10.1186/scrt171.

Circulation Research, 116(9), 1561–1578. https://doi.org/10.1161/circresaha.115.303565.

21. Long, C. A., Timmins, L. H., Koutakis, P., Goodchild, T. T., Lefer, D. J., Pipinos, I. I., et al. (2016). An endovascular model of ischemic myopathy from peripheral arterial disease. *Journal of Vascular Surgery*. https://doi.org/10.1016/j.jvs.2016.07.127.

22. Burkhardt, G. E., Gifford, S. M., Propper, B., Spencer, J. R., Williams, K., Jones, L., et al. (2011). The impact of ischemic intervals on neuromuscular recovery in a porcine (Sus scrofa) survival model of extremity vascular injury. *Journal of Vascular Surgery, 53*(1), 165–173. https://doi.org/10.1016/j.jvs.2010.07.012.

23. Grundmann, S., Hoefer, I., Ulusans, S., Bode, C., Oesterle, S., Tijssen, J. G., et al. (2006). Granulocyte-macrophage colony-stimulating factor stimulates arteriogenesis in a pig model of peripheral artery disease using clinically applicable infusion pumps. *Journal of Vascular Surgery, 43*(6), 1263–1269. https://doi.org/10.1016/j.jvs.2006.02.049.

24. Voskuil, M., van Royen, N., Hoefer, I. E., Seidler, R., Guth, B. D., Bode, C., et al. (2003). Modulation of collateral artery growth in a porcine hindlimb ligation model using MCP-1. *American Journal of Physiology - Heart and Circulatory Physiology, 284*(4), H1422–H1428. https://doi.org/10.1152/ajpheart.00506.2002.

25. Muhs, A., Lenter, M. C., Seidler, R. W., Zweigerdt, R., Kirchengast, M., Weser, R., et al. (2004). Nonviral monocyte chemoattractant protein-1 gene transfer improves arteriogenesis after femoral artery occlusion. *Gene Therapy, 11*(23), 1685–1693.

26. Stacy, M. R., Yu, D. Y., Maxfield, M. W., Jaba, I. M., Jozwik, B. P., Zhuang, Z. W., et al. (2014). Multimodality imaging approach for serial assessment of regional changes in lower extremity arteriogenesis and tissue perfusion in a porcine model of peripheral arterial disease. *Circulation. Cardiovascular Imaging, 7*(1), 92–99. https://doi.org/10.1161/circimaging.113.000884.

27. Gao, Y., Aravind, S., Patel, N. S., Fuglestad, M. A., Ungar, J. S., Mietus, C. J., et al. (2020). Collateral development and arteriogenesis in hindlimbs of swine after ligation of arterial inflow. *The Journal of Surgical Research, 249*, 168–179. https://doi.org/10.1016/j.jss.2019.12.005.

28. Landázuri, N., Levit, R. D., Joseph, G., Ortega-Legaspi, J. M., Flores, C. A., Weiss, D., et al. (2016). Alginate microencapsulation of human mesenchymal stem cells as a strategy to enhance paracrine-mediated vascular recovery after hindlimb ischaemia. *Journal of Tissue Engineering and Regenerative Medicine, 10*(3), 222–232. https://doi.org/10.1002/term.1680.

29. Krueger, T. E. G., Thorek, D. L. J., Denmeade, S. R., Isaacs, J. T., & Brennen, W. N. (2018). Concise review: mesenchymal stem cell-based drug delivery: the good, the bad, the ugly, and the promise. *Stem Cells Translational Medicine, 7*(9), 651–663. https://doi.org/10.1002/sctm.18-0024.

30. Gyöngyösi, M., Blanco, J., Marian, T., Trón, L., Petneházy, Ö., Petrasi, Z., et al. (2008). Serial noninvasive in vivo positron emission tomographic tracking of percutaneously intramyocardially injected autologous porcine mesenchymal stem cells modified for transgene reporter gene rxpression. *Circulation. Cardiovascular Imaging, 1*(2), 94–103. https://doi.org/10.1161/circimaging.108.797449.

31. Gibson, C. M., Ryan, K., Sparano, A., Moynihan, J. L., Rizzo, M., Kelley, M., et al. (1999). Angiographic methods to assess human coronary angiogenesis. *American Heart Journal, 137*(1), 169–179. https://doi.org/10.1016/S0002-8703(99)70473-4.

32. Powers, K. M., Schimmel, C., Glenny, R. W., & Bernards, C. M. (1999). Cerebral blood flow determinations using fluorescent microspheres: variations on the sedimentation method validated. *Journal of Neuroscience Methods, 87*(2), 159–165.

33. Wen, Y., Murach, K. A., Vechetti Jr., I. J., Fry, C. S., Vickery, C., Peterson, C. A., et al. (2018). MyoVision: software for automated high-content analysis of skeletal muscle immunohistochemistry. *Journal of Applied Physiology (Bethesda, MD: 1985), 124*(1), 40–51. https://doi.org/10.1152/japplphysiol.00762.2017.

34. Rotstein, B. H., Stephenson, N. A., Vasdev, N., & Liang, S. H. (2014). Spirocyclic hypervalent iodine(III)-mediated radiofluorination of non-activated and hindered aromatics. *Nature Communications, 5*, 4365. https://doi.org/10.1038/ncomms5365.

35. Rotstein, B. H., Wang, L., Liu, R. Y., Patteson, J., Kwan, E. E., Vasdev, N., et al. (2016). Mechanistic studies and radiofluorination of structurally diverse pharmaceuticals with spirocyclic iodonium(III) Ylides. *Chemical Science, 7*(7), 4407–4417. https://doi.org/10.1039/c6sc00197a.

36. Moroz, M. A., Zhang, H., Lee, J., Moroz, E., Zurita, J., Shenker, L., et al. (2015). Comparative analysis of T cell imaging with human nuclear reporter genes. *Journal of nuclear medicine : official publication, Society of Nuclear Medicine, 56*(7), 1055–1060. https://doi.org/10.2967/jnumed.115.159855.

37. Pandit-Taskar, N., Zanzonico, P., Staton, K. D., Carrasquillo, J. A., Reidy-Lagunes, D., Lyashchenko, S., et al. (2018). Biodistribution and dosimetry of (18)F-meta-fluorobenzylguanidine: a first-in-human PET/CT imaging study of patients with neuroendocrine malignancies. *Journal of Nuclear Medicine, 59*(1), 147–153. https://doi.org/10.2967/jnumed.117.193169.

38. Koutakis, P., Myers, S. A., Cluff, K., Ha, D. M., Haynatzki, G., McComb, R. D., et al. (2015). Abnormal myofiber morphology and limb dysfunction in claudication. *The Journal of Surgical Research, 196*(1), 172–179. https://doi.org/10.1016/j.jss.2015.02.011.

39. Kakihana, T., Ito, O., Sekiguchi, Y., Ito, D., Goto, H., Akamatsu, D., et al. (2017). Hip flexor muscle dysfunction during walking at self-selected and fast speed in patients with aortoiliac peripheral arterial disease. *Journal of Vascular Surgery, 66*(2), 523–532. https://doi.org/10.1016/j.jvs.2017.03.421.

40. Kaiser, E. E., Waters, E. S., Fagan, M. M., Scheulin, K. M., Platt, S. R., Jeon, J. H., et al. (2020). Characterization of tissue and functional deficits in a clinically translational pig model of acute ischemic stroke. *Brain Research, 1736*, 146778. https://doi.org/10.1016/j.brainres.2020.146778.

41. Hedayat, A. F., Park, K. H., Kwon, T. G., Woollard, J. R., Jiang, K., Carlson, D. F., et al. (2018). Peripheral vascular atherosclerosis in a novel PCSK9 gain-of-function mutant Ossabaw miniature pig model. *Translational Research, 192*, 30–45. https://doi.org/10.1016/j.trsl.2017.10.007.

42. Heinonen, I., Kemppainen, J., Kaskinoro, K., Peltonen, J. E., Borra, R., Lindroos, M. M., et al. (2010). Comparison of exogenous adenosine and voluntary exercise on human skeletal muscle perfusion and perfusion heterogeneity. *Journal of Applied Physiology (Bethesda, MD: 1985), 108*(2), 378–386. https://doi.org/10.1152/japplphysiol.00745.2009.

43. Armstrong, R. B., Delp, M. D., Goljan, E. F., & Laughlin, M. H. (1987). Distribution of blood flow in muscles of miniature swine during exercise. *Journal of Applied Physiology (Bethesda, MD: 1985), 62*(3), 1285–1298. https://doi.org/10.1152/jappl.1987.62.3.1285.

44. Varu, V. N., Hogg, M. E., & Kibbe, M. R. (2010). Critical limb ischemia. *Journal of Vascular Surgery, 51*(1), 230–241. https://doi.org/10.1016/j.jvs.2009.08.073.

45. Kościński, K., Kozłowska-Rajewicz, A., Górecki, M. T., Kamyczek, M., & Różycki, M. (2009). Month-of-birth effect on further body size in a pig model. *HOMO, 60*(2), 159–183. https://doi.org/10.1016/j.jchb.2008.02.003.

46. Dubreuil, P., Pelletier, G., Petitclerc, D., Lapierre, H., Couture, Y., Brazeau, P., et al. (1987). Influence of age and sex on basal secretion of growth hormone (GH) and on GH-induced release by porcine GH-releasing factor pGRF(1–29NH2) in growing pigs. *Domestic Animal Endocrinology, 4*(4), 299–307. https://doi.org/10.1016/0739-7240(87)90026-9.

47. Caicedo, D., Devesa, P., Alvarez, C. V., & Devesa, J. (2020). Why should growth hormone (GH) be considered a promising

therapeutic agent for arteriogenesis? Insights from the GHAS trial. *Cells, 9*(4). https://doi.org/10.3390/cells9040807.

48. Erman, A., Wabitsch, M., & Goodyer, C. G. (2011). Human growth hormone receptor (GHR) expression in obesity: II. Regulation of the human GHR gene by obesity-related factors. *International Journal of Obesity, 35*(12), 1520–1529. https://doi.org/10.1038/ijo.2011.10.

49. van der Bogt, K. E., Hellingman, A. A., Lijkwan, M. A., Bos, E. J., de Vries, M. R., van Rappard, J. R., et al. (2012). Molecular imaging of bone marrow mononuclear cell survival and homing in murine peripheral artery disease. *JACC: Cardiovascular Imaging, 5*(1), 46–55. https://doi.org/10.1016/j.jcmg.2011.07.011.